Models of Micellar Structure Tested by SANS and SAXS (from a Kratky Camera) in Cesium Dodecyl Sulfate Solution

Sz. Vass,*,† J. Pleštil,‡ P. Laggner,§ T. Gilányi,|| S. Borbély,⊥ M. Kriechbaum,§ Gy. Jákli,† Z. Décsy,# and P. M. Abuja§

KFKI Atomic Energy Research Institute, P.O. Box 49, H-1525 Budapest Hungary, Institute of Macromolecular Chemistry, 2 Heyrovsky Sq., 16202, Prague, Czech Republic, Institute of Biophysics and X-ray Structure Research, 6 Schmiedlstrasse A-8042 Graz, Austria, Departmentof Colloid Chemistry, Eötvös Loránd University, P.O. Box 32, H-1518, Budapest, Hungary, Institute for Solid State Physics and Optics, P.O. Box 49, H-1525, Budapest, Hungary, and Veterinary and Food Control Station of Veszprém County, H-8200, Veszprém, Hungary

Received: April 25, 2003; In Final Form: August 1, 2003

Small-angle neutron- (SANS) and X-ray-scattering (SAXS) patterns obtained at 40 °C from 0.0729 ***m*** D_2O solution of cesium dodecyl sulfate (CsDDS) have been simultaneously evaluated in terms of the conventional two-shell model, a three-shell model created for demonstration purposes, and a newly developed—and partly tested—four-component model. The simultaneous fitting is based on the fact that the two types of coherent scattering patterns differ only in the neutron- and X-ray scattering lengths. For comparison, the SANS and SAXS patterns were evaluated separately, too. In contrast to the two- and three-shell models, the four-component model is able to represent the continuously varying spatial distribution of the scattering contrast. From the results, it seems that the most reliable data are obtained from fitting the four-component model simultaneously to both patterns. Along with (approximate) core- and counterion profiles, application of the latter model can result in the spatial distribution of the solvent molecules around the micellar center. If an atom or a molecular group has well-distinguishable scattering contrast relative to both types of scattering (such as Cs^+ counter-, and -SO_4^-- headgroup-ions), utilization of the four-component model enables their molecular volumes to be treated as variable model parameters, thus providing a unique method for determining their hydration properties in a structured nonsimple liquid.

1. Introduction

Interpretation of scattering experiments on micellar systems is based on micelles being individual scattering entities. Every micelle contributes to the interference pattern by an elementary amplitude $A_j(Q,r_j) = \exp[-i\boldsymbol{Q}\boldsymbol{r}_j]A_j(Q)$; here $\boldsymbol{Q}$ is the change in the wave vector, $\boldsymbol{r}_j$ is the position of the micelle, and $A_j(Q) = \int \Delta\rho_j(\boldsymbol{u})\exp[-i\boldsymbol{Q}\boldsymbol{u}]\mathrm{d}\boldsymbol{u}$ is the Fourier transform of $\Delta\rho_j(\boldsymbol{u})$, the scattering contrast function distributed over micelle j. The coherent scattering cross section $\mathrm{d}\Sigma/\mathrm{d}\Omega$ (which is related—after collimation distortion—to the experimental scattering intensity converted to absolute units) is obtained by averaging the squared sum of the elementary amplitudes. By taking it into account that $A_j(Q)$'s are uncorrelated with the micellar positions, one arrives at the frequently used formula

$$\frac{\mathrm{d}\Sigma}{\mathrm{d}\Omega} = n_{\mathrm{mic}} \cdot (\langle |A(Q)|^2\rangle - \langle |A(Q)|\rangle^2 + \langle |A(Q)|\rangle^2 \cdot \langle \sum_{\mathrm{j,k}} \exp(-i \cdot \mathbf{Q} \cdot (\mathbf{r}_{\mathrm{j}} - \mathbf{r}_{\mathrm{k}}))\rangle) \quad (1a)$$

where n_{mic} is the number of micelles per unit volume and $\boldsymbol{Q} \cdot (\boldsymbol{r}_j - \boldsymbol{r}_k)$ is the phase shift of the wave between micelles j and k. The notation $\langle |A(Q)|\rangle^2$ stands for the form factor, the expression $\langle |A(Q)|^2\rangle - \langle |A(Q)|\rangle^2$ for its fluctuations, and these two quantities depend only on the arrangement of the micelle forming- and solute molecules. The mean value of the sum of the exponentials on the right-hand side of eq 1a is the structure factor denoted by $S(Q)$. It is determined by the interactions between the micelles; if the interactions are central and act pairwise, $S(Q)$ can be reduced to the Fourier transform of $g_{\mathrm{mic}}(\boldsymbol{r})$, the pair-correlation function of the micelles as

$$\langle \sum_{j,k} \exp(-i \cdot \boldsymbol{Q} \cdot (\boldsymbol{r}_j - \boldsymbol{r}_k))\rangle = \int g_{\mathrm{mic}}(\boldsymbol{u}) \cdot \exp[-i \cdot \boldsymbol{Q} \cdot \boldsymbol{u}] \cdot \mathrm{d}\boldsymbol{u} = S(Q) \quad (1b)$$

Interpretation of the experimental data requires extensive modeling of the form- and structure factors because of the nature of the quantities on the right-hand side of eq 1a. Micellar structure has always been treated in terms of (two-)shell models,[1] i.e., the micelle is divided into concentric spheroid regions within which the scattering contrast has constant, though not equal, values. In practice, so far as we are aware, the number of shells has never been greater than two. This crude approximation to the micellar structure proved to be effective, because almost every study published on micellar structure uses neutron scattering, and in this case, the experimental information originates mainly from the compact, and almost homogeneous, micellar cores. A further reason for the success of the two-

* To whom correspondence should be addressed. Tel.: 36 1 392 2299. Fax: 36 1392 2222.
† KFKI Atomic Energy Research Institute.
‡ Institute of Macromolecular Chemistry.
§ Institute of Biophysics and X-ray Structure Research.
|| Eötvös Loránd University.
⊥ Institute for Solid State Physics and Optics.
Veterinary and Food Control Station of Veszprém County.

10.1021/jp030515n CCC: $25.00
Published on Web 10/18/2003

shell model is that the volume of the core-forming molecular groups, and consequently, their scattering contrast, can be reliably calculated from precise density measurements.[2] Under these conditions, the two-shell model can accurately predict the trend of core radius R_c versus alkyl chain length.[3]

Earlier, we had attempted to improve the modeling of the structure of micelles by introducing a multi(four)-component approach instead of shell models.[4] In this approach, the surfactants are divided into characteristic molecular groups (of constant scattering property), and for each type of group, a function $\varphi_j(\boldsymbol{r})$ is defined, which stands for the probability density of finding that group in position $\boldsymbol{r}$ with respect to the micellar center. The scattering amplitude $A(Q)$ produced by a micelle is given as the linear combination of the elementary scattering amplitudes $a_i(Q)$ stemming from the characteristic groups

$$A(Q) = \sum_j a_j(Q) = \sum_j \Delta b_j n_j \int \varphi_j(r) \cdot \exp[-iQ \cdot r] \cdot \mathrm{d}r \quad (1c)$$

where Δb_j is the excess scattering length and n_j is the number of molecular group j. For spherical micelles formed from ionic surfactants one can find empirical formulas for the spatial probability density functions which, along with describing satisfactorily the micellar structure, have analytical Fourier transforms. The results obtained from utilizing the model allowed us to derive a more detailed picture of sodium alkyl sulfate micelles.[4]

Regarding the structure factor, the main problem is the type of interaction considered in micellar solutions. On the basis of previous practice,[1,3] the one-component macrofluid model[1,5] (OCM) is used in the present work. In the OCM, the micelles are thin electric double-layers immersed in a structurless medium and interact via the Deryaguin−Landau−Verwey−Overbeek (DLVO) potential[6]

$$U(r) = 2 \cdot U_0 \cdot \frac{\exp(-\kappa \cdot R_0 \cdot (r/R_0 - 2))}{r/R_0} \quad (2)$$

where U_0 is the potential strength, R_0 is the radius of the double-layers, and κ is the inverse scaling length of the electrostatic field as obtained from the Debye−Hückel theory at the critical concentration of micelle formation.[7] When calculating the $S(Q)$, the condition of impermeability $U(r) = \infty$ for $r < 2 \cdot R_0$ is added to the potential function. A very attractive feature of the DLVO potential is that $S(Q)$ is obtained in analytical form;[8] the applicability of the DLVO potential is discussed in detail in ref 3.

Because scattering curves are registered in a finite Q-range, the information available is not sufficient for inverting the Fourier transform (i.e., for uniquely determining $\Delta\rho(\boldsymbol{r})$). For this reason, the number n_P of free fitting parameters is restricted to $n_P \sim Q_{max}D_{max}/\pi$, where Q_{max} is the upper limit of the Q-range with useful scattering data and D_{max} is the maximum dimension of the particles studied.[9] In a previous study of sodium alkyl sulfate micelles,[3] the two-shell model was used to interpret scattering patterns in the range $Q < 4.8$ nm^{-1}. The core of sodium dodecyl sulfate (SDDS) micelles was found to be an ellipsoid of radius ~1.6 nm and of axial ratio ~1.6. A numerical Poisson−Boltzmann analysis[10] predicts that the thickness of the ionic shell of SDDS micelles is between $3 \cdot R_{ion}$ and $5 \cdot R_{ion}$, where R_{ion} is the counterion radius. Despite all the ambiguities stemming from the definition and determination of the ion radius, the approach in ref 10 yields Na^+ counterions less than 1 nm in shell thickness, leading to $D_{max} \approx 7$ nm and $n_P < 10-11$.

The finiteness of the Q-range is only one of the reasons that may cause difficulties in determining micellar structure from SAS; poor statistics or weak scattering contrast also decrease the reliability of certain model parameters. For example, if sodium alkyl sulfate micelles are studied by SANS, the model parameters related to the core will be determined with smaller parameter errors than those related to the ionic shell—if the latter parameters can be determined at all.[3,4] Provided that the same system is studied by SAXS, the error bars of the fitting parameters standing for the ionic shell are expected to decrease. The best-defined parameter values are expected if both SANS and SAXS patterns are considered in the interpretation,[11] and thanks to the independent neutron- and X-ray scattering mechanism, the maximum number n_P of free fitting parameters will be doubled, thus making it possible to elaborate a more refined micellar model.

The aim of the paper is to make one step in the direction of improving our knowledge of micellar structure. To this end, a selected micellar system (cesium dodecyl sulfate, CsDDS) has been studied both by SANS and SAXS. With regard to the micellar structure, the spherical multi(four)-component model has been generalized for ellipsoid micelles. To provide a general survey, along with the generalized multi(four)-component (4C) model, the two-shell (2S) model and a three-shell (3S) model were used; the last of these was for testing the effect of the increase in the number of shells on the reliability of the best-fit parameter values. The structure factor was calculated from the OCM as published in ref 3. The scattering patterns were interpreted both separately and simultaneously,[11] each in terms of all three models. By utilization of the improved experimental information, the actual volume of the headgroup- and counterions was also determined.

2. Materials and Methods

2.1. Experimental. Great care was taken in choosing the system to be studied to avoid experimental difficulties as far as possible. The critical concentration c_m of ionic surfactants decreases exponentially with the number of carbon atoms in the alkyl chain,[12,13] and for alkyl sulfates, it falls within the characteristic range of $10^{-3} - 10^{-1}$ mol/dm^3 at room temperature. To obtain a spheroid micellar shape whose axial ratio is not far from unity at small, though treatable, surfactant concentrations, a dodecyl sulfate salt was chosen. To increase both neutron and X-ray[14] scattering contrast of the counterions, the usual sodium counterion was replaced by cesium.

CsDDS was prepared from 99+% dodecyl alcohol (Aldrich) by sulfation with chlorosulfonic acid (MERCK) at 0−5 °C, such that the salt was recrystallized twice from hot 1:1 benzene/ethanol mixtures.[15] Gas chromatographic-, combined liquid chromatographic- and mass spectrometric analysis of the product showed $\sim 3 \cdot 10^{-5}$ mole fraction alcohol; the sum of all other impurities was of a similar amount. The critical concentration was determined from the specific conductivity versus concentration curve by linear extrapolation,[12] and $c_m = 0.0061 \pm 0.0005$ mol/dm^3 was obtained in D_2O at 40 °C. The reason for applying the higher, 40 °C, standard temperature is that the Krafft point for CsDDS is above 25 °C. The solution was prepared from dried (for 72 h at 55 °C) salt and from bidistilled 99.59% D_2O. Solute aquamolality was fixed at 0.0729 $\boldsymbol{m}$ (aquamolality, $\boldsymbol{m}$, gives mol of solute per 55.51 mol of isotopic water); in this range, the molar concentration c exhibits only a slight deviation from $\boldsymbol{m}$.

SANS measurements were carried out in the Budapest Neutron Center at 40 ± 0.5 °C in pinhole geometry. The mean

wavelength λ was set to 0.355 nm by a velocity selector producing neutrons with an approximately Gaussian wavelength distribution and a resolution $\Delta\lambda/\lambda \approx 12\%$ independent of λ. Neutrons were detected by a 64 × 64 pixel two-dimensional position-sensitive detector; the applied Q range was 0.1−4.8 nm^{-1}. Raw scattering patterns were circularly averaged around the primary beam location and corrected for background; they were converted into absolute units $d\Sigma_{exp}/d\Omega$ using a 1-mm thick H_2O standard. To correctly subtract the background caused by the incoherent scattering of H atoms, a H_2O/D_2O mixture was made that consisted of the same amount of hydrogen as the dissolved surfactant.

SAXS experiments were carried out on the same solution at the same temperature in the Institute of Biophysics and X-ray Structure Research, Graz, using a compact Kratky camera (MBG, Austria) attached to a rotating-anode X-ray generator (RIGAKU-DENKI, Japan) that produced Ni-filtered Cu Kα rays; the camera was equipped with a one-dimensional position-sensitive detector (MBRAUN, Germany). The values of Q varied in the range 0.1−6.0 nm^{-1}. Experimental scattering curves $I(Q)$ were first converted to absolute experimental (smeared) intensities $d\Sigma_{exp}/d\Omega$ by means of a LUPOLEN standard

$$\frac{d\Sigma_{exp}}{d\Omega} = \frac{a_{sd} \cdot I(Q)}{I_L \cdot K_L \cdot \tau \cdot \Delta D} \tag{3}$$

where a_{sd} is the sample-to-detector distance, I_L is the intensity of radiation scattered by the standard at $Q_L = (2\pi/15)$ nm^{-1}, K_L (=71.3) is a dimensionless calibration constant, and τ and ΔD are sample transmission and thickness,[16] respectively. Values of ΔD were determined from experimental τ data by making use of tabulated atomic absorption coefficients and of solution densities; the latter quantities were obtained from inter- or extrapolating available density data.[2] The incoherent background was removed by subtracting the scattering pattern from a Cs_2SO_4 solution.

2.2. The Micellar Model and the Fitting Functions. The micellar model is an approximate analytic form for the (mean) spatial distribution $\Delta\rho_j(\boldsymbol{r})$ of the scattering contrast, basically determined by the conformation of micelles. On the basis of the thermodynamic consideration[17,18] that the cores consist entirely of portions of the hydrocarbon chains, a single micelle immersed in an isotropic medium is expected to form a sphere. The aggregation number of such a micelle is determined by the alkyl chain length and turns out to be significantly less than the actual experimentally determined value. The hydrocarbon chains in micelles with realistic aggregation numbers can fit the above spatial constraints only if the micellar shape is no longer a sphere. In solutions of ionic micelles, the local electrostatic field may distort the spherical conformation, promoting the formation of prolate or oblate ellipsoids.[18,19] Because no holes may exist within the micelle, the hydrocarbon chain length should limit at least one micellar dimension.

It is pointed out that recent experimental methods are ambiguous in this respect in that the results they provide are compatible with each of the above given types of micellar shape. A high-resolution SANS study[20] of 2% (∼0.07 ***m***) SDDS solution, made on different spectrometers up to unusually high (∼10 nm^{-1}) Q values, concludes that SDDS micelles are spheres or spheroids whose axial ratio is near to unity. In a recently published work,[4] a similar conclusion has been drawn for sodium nonyl- (SNS), decyl- (SDeS), and undecyl sulfate (SUS) micelles in 0.073 ***m*** solutions. At higher concentration[21] and with increasing alkyl chain length,[3,21] a significantly better fit can be achieved by assuming prolate ellipsoids with an axial ratio of 1.2−1.6. The goodness of the fit can be even further improved if the micelles are taken to be oblate ellipsoids,[22] and based on thermodynamic arguments, oblate ellipsoids are predicted to be more likely than prolate ones.[18,19]

On the basis of the arguments discussed above, the micelles are assumed to be spheroids. A spheroid of radius R, axial ratio η, and homogeneously distributed excess scattering length Δb produces scattering amplitude A_{sph} in accordance with

$$A_{sph}(t) = \Delta b \cdot 3 \cdot \frac{\sin(QRt) - (QRt) \cdot \cos(QRt)}{(QRt)^3} \tag{4}$$

with the notation $t(\eta,\vartheta) = (1+(\eta^2\text{-}1)\cos^2(\vartheta))^{1/2}$, where ϑ is the angle between $\boldsymbol{Q}$ and the axis of symmetry of the spheroid. For $\eta = 1$, we have $t = 1$, and eq 4 becomes the well-known formula for the scattering amplitude from homogeneous spheres. Shell models are based on the assumption that the spatial symmetry of the scattering contrast distribution follows that of the micellar core.

By dividing now the scatterer into N similar, concentric, shells of outer radius R_j and scattering length density ρ_j by expressing the excess scattering length of the j-th spheroid in terms of its volume $V_j = 4 \cdot \pi \cdot R_j^3 \cdot \eta/3$ and scattering contrast $\Delta\rho_j = \rho_j - \rho_s$, the N-shell model predicts the scattering amplitude from a single micelle in the form

$$A(Q,t(\eta,\vartheta)) = \sum_{j=1}^{N} (\Delta\rho_{j+1} - \Delta\rho_j) \cdot V_j \cdot 3 \cdot \frac{\sin(QR_jt(\eta,\vartheta)) - (QR_jt(\eta,\vartheta))\cos(QR_jt(\eta,\vartheta))}{(QR_jt(\eta,\vartheta))^3} \tag{5}$$

where $\rho_{N+1} \equiv \rho_s$ is the scattering length density and $\Delta\rho_{N+1} = 0$ is the scattering contrast of the bulk solvent. The first and second moments of the scattering amplitude in eq 4 are given by the integrals

$$\langle A(Q,\eta)\rangle = \frac{1}{2}\int_0^\pi A(Q,t(\eta,\vartheta)) \sin(\vartheta)\, d\vartheta \tag{6a}$$

and

$$\langle A^2(Q,\eta)\rangle = \frac{1}{2}\int_0^\pi A^2(Q,t(\eta,\vartheta)) \sin(\vartheta)\, d\vartheta \tag{6b}$$

2.2.1. Two- (2S) and Three-Shell (3S) Models. If the variables of eq 5 are fitting parameters, the poor information content of the scattering pattern limits the number of the shells to N = 2−3. The innermost shell of radius $R_1 = R_c$ stands for the micellar core; the axial ratio is determined from the equation $4\pi \cdot R_c^3 \cdot \eta/3 = n_{ag} \cdot v_{alk}$. Because the core is assumed to be compact and to contain no water,[2,3,21] its scattering contrast is simply $\Delta\rho_1 = \Delta\rho_c \approx \Delta b_{alk}/v_{alk}$, where $\Delta b_{alk} = b_{alk} - \rho_s v_{alk}$, v_{alk} is the volume of the alkyl chain,[2] and b_{alk} is the corresponding scattering length taken from a standard table.[23] If two shells are assumed, $R_2 = R_{sh}$ is the outer radius of the ionic sphere and its scattering contrast is given as $\Delta\rho_2 = \Delta\rho_{sh} = 3n_{ag}(\Delta b_{SO4} + \Delta b_M)/(4\pi(R_{sh}^3 - R_c^3)\eta)$, with the excess scattering length $\Delta b_{SO_4} = b_{SO_4} - \rho_s v_{SO_4}$ of the headgroup-, and $\Delta b_M = b_M - \rho_s v_M$ of the counterions. Ionic volumes v_{SO_4} and

v_M are taken from Ref 24; further properties of the scattering contrast are discussed in more detail in ref 3.

In the 3S variant of eq 5, the core is defined in the same way as in the 2S model (i.e., $R_1 = R_c$ and $\Delta\rho_1 = \Delta\rho_c$). The ionic sphere is divided into two regions: the inner one of radius $R_2 = R_h$ consists of the headgroup-ions and a fraction β of the counterions. Here, the contrast equals $\Delta\rho_2 = \Delta\rho_h = 3n_{ag}(\Delta b_{SO_4} + \beta\Delta b_M)/(4\pi(R_h^3 - R_c^3)\eta)$. The fraction $(1 - \beta)$ of the counterions is found within the third, outermost, shell of radius $R_3 = R_{sh}$; these counterions cause a scattering contrast $\Delta\rho_3 = \Delta\rho_{sh} = 3n_{ag}(1 - \beta)\,\Delta b_M/(4\pi(R_{sh}^3 - R_h^3)\eta)$.

2.2.2. Spherical Four-Component (4c) Model. The 4C model[4] focuses on the micelle-forming molecules rather than the whole micelle. It divides the (alkali alkyl sulfate) molecules into methyl- (CH_3-, $j = 1$), methylene- (CH_2-, $j = 2$), and sulfate- ($-SO_4^-$-, $j = 3$) groups as well as into counterions (M^+, $j = 4$). The hydrophobic ($-CH_3$ and $-CH_2$-) groups are assumed to have radial profiles described by the same, properly parametrized, error function

$$\varphi_j^s(r) = \frac{1}{2f_j}\left(1 - \mathrm{erf}\left(\frac{r - R_c}{\sqrt{2}\sigma_c}\right)\right) j = 1,2 \qquad (7a)$$

where R_c is the radius at which the radial density halves, σ_c defines the thickness of the core profile in the hydrocarbon/water interface. Those hydrophobic groups that are in contact with the solvent are assumed to have a Gaussian distribution, while those that are found inside the core are assumed to have an even spatial distribution. The normalization condition $\int \varphi_j(r) r^2\,\mathrm{d}r = 1$ makes f_1 and f_2 equal to the volume of the hydrocarbon microphase

$$f_j = \frac{2\pi R_c^3}{3}\left\{\left(1 + \frac{3\sigma_c^2}{R_c^2}\right)\left(1 + \mathrm{erf}\left(\frac{R_c}{\sqrt{2}\sigma_c}\right)\right) + \frac{\sqrt{2}\sigma_c}{\sqrt{\pi}R_c}\left(1 + \frac{2\sigma_c^2}{R_c^2}\right)\exp\left(-\frac{R_c^2}{2\sigma_c^2}\right)\right\}, j = 1,2 \qquad (7b)$$

The terminal methylene groups are located along the core profile such that the headgroup-ions are shifted towards the aqueous phase by Δd_h, leading to

$$\varphi_3^s(r) = \frac{1}{\sqrt{2\pi}\sigma_c f_3}\exp\left(-\left(\frac{r - R_c - \Delta d_h}{\sqrt{2}\sigma_c}\right)^2\right) \qquad (8a)$$

where $\Delta d_h = 0.296$ nm for alkyl sulfates. The normalization condition for f_3 results in

$$f_3 = \frac{(R_c + \Delta d_h)^2}{2}\left(1 + \mathrm{erf}\left(\frac{R_c + \Delta d_h}{\sqrt{2}\sigma_c}\right)\right) \qquad (8b)$$

The Poisson−Boltzmann equation predicts that the counterion distribution $\varphi_4^s(r)$ around a thin ($\sigma_c \ll R_c$) spherical shell of the headgroup-ions varies versus r, like $A \cdot \exp(B \cdot \exp(-\kappa r)/r)$, an expression without analytical Fourier transform. It was shown[4] that a suitable approximation to the exact solution of the Poisson−Boltzmann equation can be achieved by a simple exponential $\exp(-\Lambda r)$. The effect of a wide ($\sigma_c \approx R_c$) spatial distribution of the micellar charge on the counterion profile is considered by convoluting $\exp(-\Lambda r)$ with the spatial density function of the headgroups

$$\varphi_4^s(r) = \frac{\Lambda}{\sqrt{2\pi}\sigma_c f_4}\int_0^r \exp\left(-\left(\frac{t - R_c + \Delta d_h}{\sqrt{2}\pi_c}\right)^2 - \Lambda(r - t)\right)\mathrm{d}t = \frac{\Lambda}{2f_4}\exp\left(\frac{\Lambda^2\sigma_c^2}{2} - \Lambda(r - R_c - \Delta d_h)\right) \times \left(\mathrm{erf}\left(\frac{r - R_c - \Delta d_h - \Lambda\sigma_c^2}{\sqrt{2}\sigma_c}\right) + \mathrm{erf}\left(\frac{R_c + \Delta d_h + \Lambda\sigma_c^2}{\sqrt{2}\sigma_c}\right)\right) \qquad (9a)$$

where Λ is the damping constant of the exponential function and $1/\Lambda$ is the characteristic width of the counterion profile. From the normalization condition, we have

$$f_4 = 2\pi\left(\sigma_c\sqrt{\frac{2}{\pi}}\left(R_c + \Delta d_h + \frac{1}{\Lambda}\right)\exp\left(-\frac{(R_c + \Delta d_h)^2}{2\sigma_c^2}\right) + \left(1 + \mathrm{erf}\left(\frac{R_c + \Delta d_h}{\sqrt{2}\sigma_c}\right)\right)\left(\left(R_c + \Delta d_h + \frac{1}{\Lambda}\right)^2 + \frac{1}{\Lambda^2} + \sigma_c^2\right)\right) \qquad (9b)$$

To calculate the scattering contrast, one has to consider the distribution $\varphi_s^s(r)$ of solvent molecules, too. Due to the incompressibility of liquids, the probability density functions satisfy the identity $v_s n_s \varphi_s^s(r) + \sum_{j=1}^4 v_j n_j \varphi_j^s(r) \equiv 1$, from which one obtains $n_s\varphi_s^s(r) = 1/v_s - \sum_{j=1}^4 v_j n_j \varphi_j^s(r)/v_s$. By considering that the scattering length density ρ_j from group j equals $b_j n_j \varphi_j(r)$ and that ρ_s from the (bulk) solvent equals b_s/v_s, the continuously varying scattering contrast $\Delta\rho_{mic}(r) = \rho_{mic}(r) - \rho_s$ from the micelle is expressed as $\sum_{j=1}^4 \Delta b_j n_j \varphi_j^s(r)$, where $\Delta b_j = (b_j - v_j\rho_s)$.

The Fourier transform of $\Delta\rho_{mic}(r)$ gives the elementary scattering amplitude $A(Q)$ from a micelle. By introducing the notation $a_j(Q) = \int n_j\varphi_j(\boldsymbol{r})\,\exp(-i\boldsymbol{Q}\cdot\boldsymbol{r})\,\mathrm{d}\boldsymbol{r}$, the elementary scattering amplitude from a micele can be given as $A(Q) = \sum_{j=1}^4 \Delta b_j a_j(Q)$, a linear combination of $a_j(Q)$, $j = 1,...4$, the Fourier transforms of the functions $n_j\varphi_j(r)$, cf. eq 1c. Provided that φ_j's are taken from eqs 7a, 8a, and 9a, the Fourier transforms can be presented in analytical form;[4] the use of the superscript s in eqs 7a, 8a, and 9a emphasizes that the above formulas are valid for micelles with spherical symmetry.

2.2.3. Generalization of the Spherical 4C Model for Ellipsoids. Generalization of the spherical model for ellipsoids is made possible by assuming that the spherical model describes the variation of the scattering contrast in the plane of the semiminor axis (for prolate ellipsoids) or in the plane of the semimajor axis (for oblate ellipsoids).[25] Let us now define an ellipsoid of radius $R_{max} = R_c + \Delta d_h + 3/\Lambda$ and then divide the interval $[0,R_{max}]$ into N, not necessarily equal, subintervals $[R_{k-1},R_k]$, $k = 1,...N$, each defining a similar, concentric shell. Within shell k, the probability density φ_{jk} of finding a particular group of type j is defined in terms of the spherical functions as

$$\varphi_{jk} = \frac{1}{2}(\varphi_j^s(R_{k-1}) + \varphi_j^s(R_k)), \quad k = 1,2,..N, \quad \text{and } R_0 = 0 \qquad (10a)$$

The axial ratio η is defined by the volume f_1 (or f_2) of the hydrocarbon microphase of the reference spherical micelle and the actual volume $n_{ag}v_{alk}$

$$\eta = \frac{n_{ag}\nu_{alk}}{f_1} \tag{10b}$$

It follows from eq 10a that $\Delta\rho_k$, the scattering contrast within shell k has the form

$$\Delta\rho_k = \rho_k - \rho = \sum_{j=1}^{4} \Delta b_j \varphi_{jk} \tag{11}$$

the scattering amplitude from a spheroid is obtained by setting eq 11 into eq 5 with the newly defined shell number N. The shape of the radial profiles is demonstrated in Figure 1.

2.3. Polydispersity Effects and the Fitting Function. Provided the scatterers are uniform, the model function is obtained by setting eqs 6a and 6b into eq 1a. The aggregation number of micelles, however, may be a random variable that makes the micelles different. On the basis of reasonable assumptions, it can be shown that the probability w_i of finding a micelle with aggregation number $n_{ag} = i$ can be well approximated by a Gaussian[26]

$$w_i(\bar{n}_{ag},\sigma_{ag}) = \frac{1}{\sqrt{2\cdot\pi}\cdot\sigma_{ag}} \cdot \exp\left(-\frac{(i-\bar{n}_{ag})^2}{2\cdot\sigma_{ag}^{\,2}}\right) \tag{12}$$

where $\bar{n}_{ag}$and σ_{ag} are the mean value and the width of the distribution, respectively.

So far as the scattering amplitude is concerned, the main question is how do the micelles change their conformation if n_{ag} changes. To provide an explanation for this, we follow the conclusions of a comprehensive dynamic light scattering study of sodium alkyl sulfates in the presence of added electrolyte.[27] This model assumes that micelles formed at cmc are spheres. When the surfactant concentration above cmc is increased, the spheres split into two hemispheres and spherical layers are embedded between them in one-molecule-thick steps, forming cylinders closed by two hemispheres. Provided that the length of the cylinders is not too long compared with the spherical radius, as in the present case, the micellar shape can be well approximated by a prolate ellipsoid. According to this assumption, the growth of micelles in the radial direction is limited by the alkyl chain length, in agreement with the conditions set in the first paragraph of Section 2.2. The key argument for using this model to interpret the scattering patterns is based on comparing core radii from a systematic SANS[3] study of sodium alkyl sulfate micelles with the alkyl chain length data stemming from independent methods. The core radii define a straight line as a function of the number n_C of carbon atoms in the alkyl chain in the range $n_C = 9-16$. Although the radii are systematically less than the length of the corresponding, expanded alkyl chains, the slope of the former is in excellent (<5%) agreement with that of the latter.

Let $A_i(Q)$ be the scattering amplitude from a micelle of aggregation number $n_{ag} = i$. The coherent scattering cross section from a polydisperse set of micelles is given by

$$\frac{d\Sigma}{d\Omega} = n_{mic}\Big(\sum_i W_i\langle A_i^2(Q)\rangle - \Big(\sum_i W_i\langle A_i(Q)\rangle\Big)^2 + \sum_i\sum_j W_i\cdot W_j\cdot\langle A_i(Q)\rangle\cdot\langle A_j(Q)\rangle\cdot S_{ij}(Q)\Big) \tag{13}$$

where $S_{ij}(Q)$ is the structure factor between micelles of aggregation numbers i and j; the quantities W_i either equal w_i or are obtained by summing up w_i in certain ranges, symmetric to the mean value $\bar{n}_{ag}$. Provided that the distribution of the micellar aggregation number is narrow, $\sigma_{ag}/\bar{n}_{ag} \ll 1$, the lengthy calculation of the whole set of $S_{ij}(Q)$'s is circumvented[28] by replacing them with a mean structure factor $\bar{S}(Q)$ calculated from the DLVO potential in eq 2. Let us introduce the mean values $\bar{A}(Q) = \Sigma_i W_i(\bar{n}_{ag},\sigma_{ag})\cdot\langle A(Q)\rangle$ and $\overline{A^2}(Q) = \Sigma_i W_i(\bar{n}_{ag},\sigma_{ag})\cdot\langle A^2(Q)\rangle$ by making use of the quantities defined in eqs 6a and 6b. With this notation, the final form of the model function is

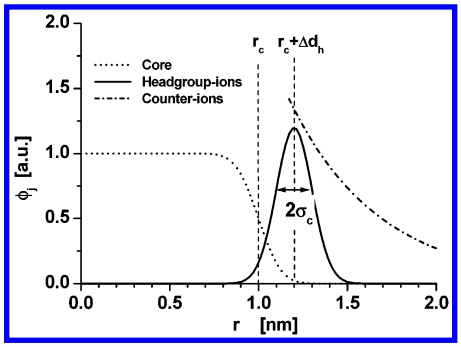

Figure 1. Spatial density functions demonstrating the likelihood of finding a particular molecular group at distance r from the (spherical) micellar center. The main merit of these functions is their ability to describe continuous material- and contrast distribution.

$$\frac{d\Sigma}{d\Omega} = n_{mic}\cdot(\overline{A^2}(Q) - \bar{A}^2(Q) + \bar{A}^2(Q)\cdot\bar{S}(Q)] \tag{14}$$

To interpret the experimental scattering intensity $d\Sigma_{exp}/d\Omega$ in terms of eq 14, one has to consider the effect of collimation distortions on the model function. This smearing effect can be formulated mathematically as a linear integral transform of $d\Sigma/d\Omega$ that strongly depends, in particular at small Q's, on the collimation geometry.[29] The fitting function is the smeared intensity $L(d\Sigma/d\Omega)$, the smearing procedures are taken from refs 29 and 30.

3. Results and Discussion

3.1. Fitting Model Functions. The parameters used in the fitting are divided into three groups, forming parameter-vectors $\boldsymbol{P}_{mic}$, $\boldsymbol{P}_{im}$ and $\boldsymbol{P}_{aux}$. The first stands for the parameters of the micellar structure[3,4] (aggregation number, polydispersity, different types of radii, profiles, volumes), the second for that of intermicellar interactions (parameters of the structure factor[3,5]); and the third for the auxiliary parameters (correction factors, additive constants, collimation parameters[29,30] $\boldsymbol{P}_{coll}$, with the latter always being fixed). Interpretation of the experiments is made in the usual way by minimizing the sum of the squared difference of experimental and smeared theoretical spectra

$$\chi^2(\mathbf{P}_{mic},\mathbf{P}_{im},\mathbf{P}_{aux}) = \sum_k \chi_k^2(\mathbf{P}_{mic},\mathbf{P}_{im},\mathbf{P}_{aux}) \tag{15a}$$

The summands in eq 15a are

$$\chi_k^2(\mathbf{P}_{mic},\mathbf{P}_{im},\mathbf{P}_{aux}) = \sum_{i_k}(d\Sigma_{exp,k}(Q_{i_k})/d\Omega - C_k\cdot L(d\Sigma(Q_{i_k};\mathbf{P}_{mic},\mathbf{P}_{im})/d\Omega,\mathbf{P}_{coll}) - B_k)^2 \tag{15b}$$

where $k = 1$ and 2 stand for SANS patterns measured at 1.3 and 5 m sample-to-detector distance, respectively, and $k = 3$ for SAXS patterns. Parameters C_k serve for correcting errors made when converting scattering patterns into absolute units, B_k serve for that made when subtracting the incoherent

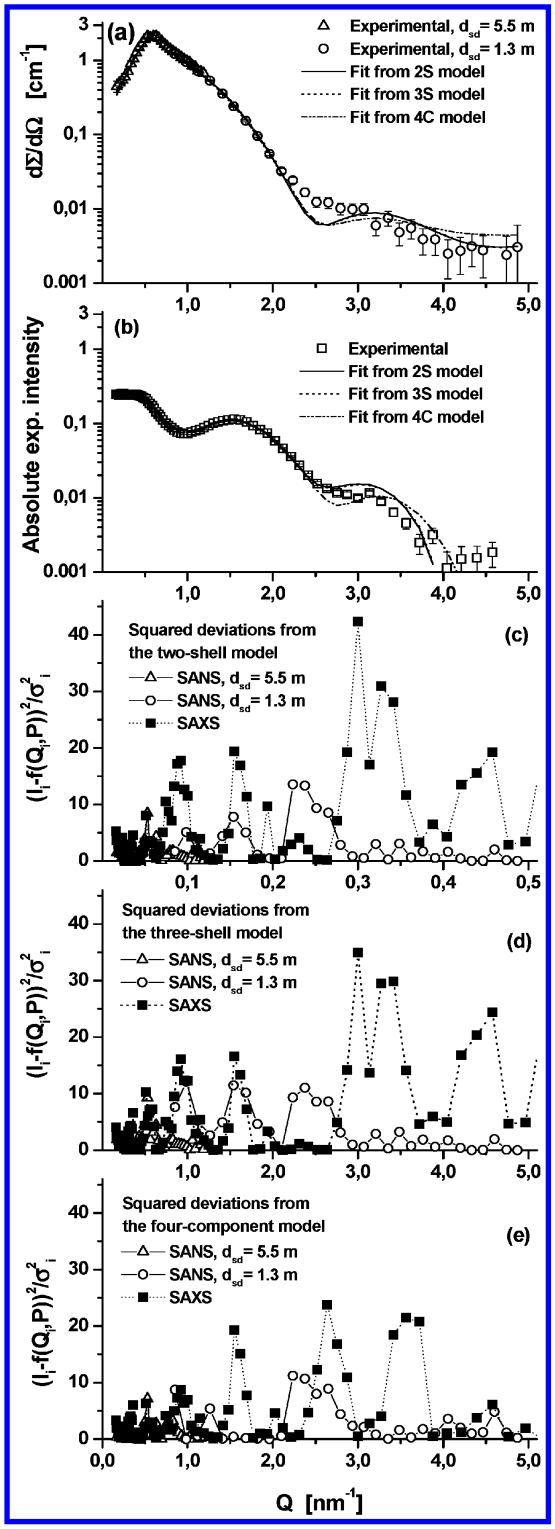

Figure 2. Best-fit curves from fitting the 2S, 3S, and 4C models to SANS (a) and SAXS (b) patterns from 0.0729 m D2O solution of CsDDS. The squared differences of the experimental data and the 2S (c), 3S (d), and 4C (e) models.

background; in the present case, $B_1 \equiv B_2$. Minimization of the sum of squares and the error analysis made use of the MINUIT package.[31]

3.2. Comparison of the Models by Analyzing CsDDS Scattering Patterns. To compare the capability and the limitations of the models, all of them were fitted to all possible combinations (SANS, SAXS, SANS + SAXS) of the scattering patterns. Due to the poor spatial resolution of the method, qualification of the models is a difficult task. The difficulty is

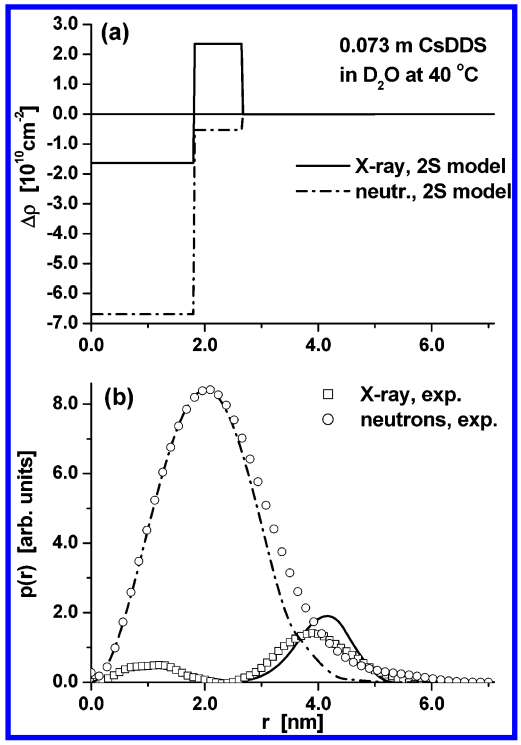

Figure 3. Radial profile of the neutron- and X-ray scattering contrast of CsDDS micelles according to the 2S model, calculated from the row-averages in Table 1 (a). Experimental *p(r)* functions obtained in a model-free way by using the ITP program[33] (b).

demonstrated in Figure 2, where the experimental data are plotted together with the best-fit curves and the squared deviations. In the range $Q < 2.0$ nm^{-1}, the best-fit curves from all the models seem to match the scattering patterns equally well, and for $Q > 2.0$ nm^{-1}, they produce similar mismatch. Apart from examining chi-squares, the ranking of the models is based on reasonable, though arbitrary, principles, like comparing the parameters and their errors with one another, and if possible, with independent results. The best-fit values of the model parameters and, where significant, their errors, are listed in Tables 1-3. Finally, the neutron- and X-ray distance distribution functions obtained from experiment and model calculations are also compared (Figures 3 and 4).

3.2.1. Parameters of the Micellar Structure. Table 1 lists the parameters of the micellar structure. From the point if view of practice, the most significant of them are the aggregation number $\bar{n}_{ag}$ and core radius R_c (they determine the axial ratio η, cf. section 2.2.1). The two parameters are strongly correlated: for the RMS errors of the row averages, we have $\Delta\bar{n}_{ag}/\bar{n}_{ag} \approx 3\Delta R_c/R_c$. As in previous studies,[3,4] the width σ_{ag} of the aggregation number distribution turned out to be poorly defined by having usually small, $\sigma_{ag} < 1$, best-fit values with large, $\Delta\sigma_{ag} > 5$, parameter errors. To test the effect of σ_{ag} on the fitting, all SANS patterns have been reevaluated under the condition $\sigma_{ag} = 0$, causing no practical change in the best-fit values of the other model parameters. This finding justifies the set of $S_{ij}(Q)$'s is being replaced in eqs 12 and 14 by a single $\bar{S}(Q)$ function.[28]

The thickness, σ_c, of the core profile has a physical significance in the 4C model only, and the results from the three scattering patterns (SANS, SAXS, SANS + SAXS) are equal within 1σ experimental error. The thickness of the hydrocarbon/water interface equals $3 \cdot \sigma_c$; it falls within the range of the spatial resolution $\pi/Q_{max} \sim 0.6-0.7$ nm. This result contradicts the narrow interface assumed in a former SANS study of SDDS micelles,[20] but is in agreement with the conclusion drawn from

TABLE 1: Best-Fit Values of the Model Parameters Standing for the Micellar Structure and Molecular Volumes from Fitting the Two-Shell- (2S), Three-shell- (3S), and Four-component (4C) Model to Single SANS- and SAXS Patterns, as Well as from Simultaneously Fitting the Models to Both Types of Scattering Pattern[a]

			SANS			SAXS			SANS + SAXS		
param	unit	row avg	2S	3S	4C	2S	3S	4C	2S	3S	4C
$\bar{n}_{ag}$		69,23	72,01	78,82	67,00	63,29	68,11	70,51	69,94	68,93	64,49
		± 1.52	5,51	2,59	1,35	2.95	1,04	4,25	1,61	1.39	1,24
R_c	[nm]	1,644	1,723	1,612	1,681	1,610	1,637	1,637	1.650	1,638	1,605
		± 0,013	0,102	0,007	0,049	0,003	0,003	0,004	0,002	0,002	0,015
σ_c	[nm]	0,242			0,181			0,291			0,254
		± 0,032			0,054			0,040			0,005
R_2-R_c	[nm]	0,851	0,513	0,901		1,001	0,901		0,898	0,891	
		± 0,070	0,161	0,163		0,006	0,005		0,003	0,027	
b		0,913		0,876			0,929			0,934	
		± 0,019		0,031			0,011			0,023	
Λ	[nm^{-1}]	2.698			1,900			3,821			2,373
		± 0,5785			0,506			1,360			0,214
R_3-R_2	[nm]	4,379		5,500			3,706			3,932	
		± 0,564		1,256			1,392			0,673	
γ_{CH3}							1,000 (fixed)				
γ_{CH2}							1,000 (fixed)				
γ_{SO4}		1.099	0,953	1,233	1,247	0,845	1,094	1,449	0,961	1,121	0.997
		± 0.066	n.s.[b]	n.s.	n.s.	n.s.	0,146	n.s.	0,167	0,070	0,035
γ_{Cs}		1.424	1,509	1,289	1,061	1,340	1,200	1,683	1,484	1,212	2.040
		± 0.099	n.s.	n.s.	n.s.	n.s.	0,129	n.s.	0,201	0,154	0,211
η		1,305	1.195	1,597	1,157	1,287	1,316	1,244	1,320	1,332	1,299
		± 0,052									

[a] Primary variables are given error bars. [b] n.s. = not significant

TABLE 2: Best-Fit Values of the Model Parameters Standing for the Interaction Potential from Fitting the Two-Shell- (2S), Three-Shell- (3S), and Four-Component (4C) Model to Single SANS- and SAXS Patterns, as Well as from Simultaneously Fitting the Models to Both Types of Scattering Pattern[a]

			SANS			SAXS			SANS+SAXS		
param	unit	row avg	2S	3S	4C	2S	3S	4C	2S	3S	4C
R_0	[nm]	3,512	4,139	3,466	4,098	3,336	3,261	3,317	3,484	3,290	3,215
		± 0,118	0,246	0,352	0,166	0,270	0,372	0,202	0,253	0,235	0,165
U_0	[k_BT]	4,941	5,216	6,311	5,597	3,612	5,175	4,559	4,272	5,141	4,587
		± 0,263	0,436	1,033	0,287	0,444	0,212	0,911	0,322	0,433	0,300
S_q	[μCcm^{-2}]	1,454	1,264	1,659	1,322	1,305	1,598	1,474	1,357	1,579	1,527
		± 0,048									
$1/\kappa$	[nm]	3,716	3,716 (fixed)								

[a] Primary variables are given error bars.

TABLE 3: Best-Fit Values of the Auxiliary Parameters from Fitting the Two-Shell- (2S), Three-shell- (3S), and Four-Component (4C) Model to Single SANS- and SAXS Patterns, as Well As From Simultaneously Fitting the Models to Both Types of Scattering Pattern[a]

			SANS			SAXS			SANS+SAXS		
param	unit	row avg	2S	3S	4C	2S	3S	4C	2S	3S	4C
C_1		1,051	1,100	1,147	0,809				1,189	1,223	0,838
		± 0,074	0,199	0,103	0,196				0,048	0,050	0,189
C_2		0,973	1,049	1,099	0,771				1,060	1,059	0,800
		± 0,060	0,055	0,224	0,184				0,030	0,028	0,180
C_3		0,946				0,867	0,927	0,980	0,887	0,934	1.081
		± 0,031				0,032	0,032	0,239	0,030	0,024	0,038
$B_1 = B_2$	[cm^{-1}]	0,0027	0,0020	0,0021	0,0034				0,0022	0,0021	0,0043
		± 0,0004	0,0018	0,0041	0,0018				0,0015	0,0014	0,0015
B_3	[cm^{-1}]	−0,0025				−0,0016	−0,0039	−0,001	−0,0035	−0,0038	−0,0010
		± 0,0006				0,0012	0,0012	0,0011	0,0010	0,0008	0,0006
χ^2_1			8,8	15,4	15,8				44,3	53,9	36,8
χ^2_2			30,2	41,0	58,5				91,6	118,3	83,4
χ^2_3						459,9	469,1	318,1	522,4	492,1	333,3
χ^2_r			0,70	1,04	1,35	5,88	6,17	4,13	4,57	4,68	3.17

[a] Primary variables are given error bars.

the application of the spherical 4C model to SNS, SDeS, and SUS micelles.[4]

In the 2S- and 3S models, the shell next to the core consists of all headgroup- and a fraction β of the counterions such that $\beta = 1$ is by definition in the 2S model. Apart from the poorly defined 2S/SANS result, the best-fit values of $R_2 - R_c$ agree surprisingly well. The value of R_2 is also in a good agreement with the hydrodynamic radius (2.5 nm) of NaDDS micelles, obtained by extrapolating to zero salt concentration the results of quasi-elastic light scattering measurements[32]. From the 3S

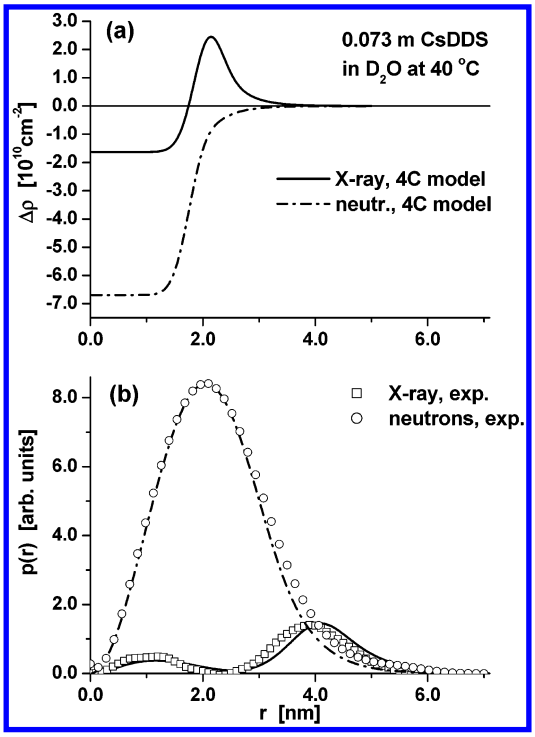

Figure 4. Radial profile of the neutron- and X-ray scattering contrast of CsDDS micelles according to the 4C model, calculated from the row-averages in Table 1 (a). Experimental *p(r)* functions obtained in a model-free way by using the ITP program[33] (b).

model $\beta \sim 0.87-0.93$ was obtained, indicating that most of the counterions are located in the vicinity of the headgroup ions. This finding was predicted by theory[10] and supports the equivalence of $R_2 - R_c$ in the two models. The thickness of the counterion profile from the 4C model equals $\sim 3/\Lambda$; its best-fit values define a row-average of 1.21 ± 0.22 nm, demonstrating a good agreement with $R_2 - R_c$ data.

The best-fit values of $R_3 - R_2$ from the 3S model indicate the presence of a wide outer ionic shell, which seems to contradict the previously discussed results. The thickness of the outer shell is determined by the scattering from a fraction $\beta \sim 0.1$ of the counterions and is poorly defined by the physical nature of the system, as reflected by the parameter errors. The presence of a wide, third shell can be interpreted either as a crude approximation to the tail of the exponential counterion distribution, or as an artifact stemming from distorted data due to improper collimation correction and/or capillary subtraction.

The conclusions drawn from model fitting can be tested by the distance distribution function $p(r) = r^2 \cdot \Delta\tilde{\rho}^2(r)$, where $\Delta\tilde{\rho}^2(r)$is the autocorrelation function of the scattering contrast $\rho(r)$ defined on the "average" micelle.[33] For X-ray patterns from a Kratky camera the ITP program[34] is the appropriate tool for determining *p(r)* in a model-free way with mathematical rigor. The results are plotted together with *p(r)* functions calculated[35] from the 2S− (Figure 3) and 4C model form factors (Figure 4). The first peak in the experimental *p(r)* function stands for the micellar core and seems to be approximated slightly better by the 2S model. The second peak stems from the ions; it—and particularly its rightmost region, which stems from the tail of the counterion profile—is matched significantly better by the 4C model. This finding supports the validity of the 4C model and of the best-fit value of Λ, the related model parameter. The same analysis has been carried out for the neutron pattern, and the results are plotted in Figures 3 and 4, too. Although the model curves acceptably match the experimental one, the conditions for X-ray- and neutron-beam collimation are essentially different, such that these results can be used only for demonstration purposes.

3.2.2. Molecular Volumes. One of the novel features of the present analysis is the attempt to consider the volumes as variable fitting parameters. In a liquid, the average space required by a certain component is defined by the intermolecular interactions, expressed by the partial molar volume V_j of the component in question. The molecular volume v_j is obtained by dividing V_j by Avogadro's number N_A. In the—simplest—case of binary systems the partial molar volume of both components depends (at constant pressure and temperature) on the composition: $V_j = V_j(m_1,m_2,p,T)$. If the system is dilute for one of the components (= solute, component 2), one may assume that the partial molar volume V_1 of the other (= solvent, component 1) remains independent of the composition and equals its bulk value. Under this condition, the molar volume of the solute is called apparent molar volume and is denoted by $V_{2\phi}$. Apparent molar volumes are determined from precise density measurements.[2] As a consequence of the Gibbs−Duhem equation, partial- and apparent quantities at molal concentration m are connected by the expression

$$V_2(m) = \frac{\mathrm{d}}{\mathrm{d}m}(mV_{2\phi}(m)) \tag{16}$$

In a micellar solution the solute is present in the form of counterions, monomer- and aggregated surfactant ions. To determine the scattering contrast, first the contributions from monomer- and aggregated surfactant ions have to be separated from one another. Then, the molecular volume of the micelle forming surfactant ions (for the multicomponent model the volumes of its segments) and that of the counterions should be determined.

The solution to this problem is based on empirical assumptions that lack any thermodynamic rigor. The apparent molar volume $V_{2\phi,\mathrm{mon}}$ of monomers and $V_{2\phi,\mathrm{agg}}$ of aggregated surfactants are assumed constant; they are separated by fitting the following equation to experimental $V_{2\phi}$ data

$$V_{2\phi} = m_c \cdot V_{2\phi,\mathrm{mon}} + (m - m_c) \cdot V_{2\phi,\mathrm{agg}} \tag{17}$$

It should be pointed out that eq (17) is very approximate, because the Gibbs−Duhem equation would require the presence of a term which depends on the logarithm of the concentration.

As a function of the number n of methylene groups, $V_{2\phi,\mathrm{agg}}$ data define a straight line, thus supporting the applicability of group-additivity[2]

$$V_{2\phi,\mathrm{agg}} = V_{n=0} + n \cdot V_{\mathrm{CH_2}}, \text{ and } V_{n=0} = V_{\mathrm{CH_3}} + V_{\mathrm{SO_4}} + V_M \tag{18}$$

where the slope equals the apparent molar volume $V_{\mathrm{CH_2}}$ of the methylene groups; $V_{n=0}$ stands for the sum of the volumes $V_{\mathrm{CH_3}}$ of the methyl groups, $V_{\mathrm{SO_4}}$ of the headgroup, and V_M of the counterions. Unlike $V_{\mathrm{CH_2}}$, which can be precisely defined by the experimental data, the terms in $V_{n=0}$ cannot be determined individually. By assuming that $V_{\mathrm{SO_4}} + V_M$ has the same value for monomer- and aggregated surfactants, a guess was made for $V_{\mathrm{CH_3}}$, leading to more or less reasonable and precise results.[2] The ionic volumes were taken from a classical paper[24] on infinite dilution molar volumes, which were corrected by the first term of Redlich's power series.

As seen from the above procedure, the scattering contrast, the basic quantity of the scattering technique, can be determined in micellar systems only in a rather arbitrary way. Poorly defined contrast leads to poor structural data, which is possibly one of

the reasons for sometimes having significantly different aggregation numbers determined from the same micellar system in different laboratories.[21,36] To the best of our knowledge, up till now, no thermodynamic method is available for deducing more reliable molecular volumes in a micellar system. One way of overcoming this problem might be to treat the molecular volumes, and thus the scattering contrast, as a variable model parameter. Because the number of variable model parameters is limited and the contrast correlates with those structural parameters due to be determined by knowing of the contrast, the fitting of molecular volumes requires special care.

In the present paper, the molecular volumes are treated as $v_j = \gamma_j \cdot v_{oj}$, where $v_{oj} = V_j/N_A$, and the molar volumes V_j are taken from refs 2 and 24. If an atom or a molecular group has a well distinguishable scattering contrast (such as Cs^+ counter-, and $-SO_4^-$- headgroup-ions with regard to both types of scattering), an attempt can be made to treat their molecular volumes as variable model parameters. All initial values of γ_j are set to equal 1; the correction factors γ_1 ($= \gamma_{CH_3}$) and γ_2 ($= \gamma_{CH_2}$) of the − assumedly precise − volumes of hydrophobic groups are fixed, the correction factors γ_3 ($= \gamma_{SO_4}$) and γ_4 ($= \gamma_M$) of the ionic volumes are variable. By fitting the three models to single- and combined SANS and SAXS patterns, the best-fit values of γ_{SO_4} vary in the range 0.8−1.5 around the average 1.099, those of γ_M in the range 1.1−1.7 around the average 1.424. Though the error bars are large enough to make most best-fit parameter values insignificant, the row-averages indicate the need to correct the counterion volume, see Table 1. Data of improved quality stem from the simultaneous fitting, suggesting that the initial value of the headgroup volume is more or less correct, and that of the counterion should be modified.

3.2.3. Parameters of the Interaction Potential. Though the best-fit values of the interaction potential parameters also vary with the model and with the type of scattering pattern, their variation is less than that of the structural parameters. Results derived here from single SANS patterns do not differ significantly from those previously obtained[3] by SANS for SDDS. By comparison of the row-averages of Table 2 with the SDDS best-fit values in ref 3, 3.51 and 3.22 nm were obtained for R_0, 4.94 and 4.54 for U_0/k_BT, and 1.45 and 1.60 $\mu C/cm^2$ for the charge density s_q on the contact surface of radius R_0, respectively, with all quantities being equal within the 1σ experimental limit. In other words, the parameters of the interaction potential acting among similar, charged particles are equal to one another. The closest approach of the micelles defined as $2 \cdot (R_0 - R_c) \approx 1.75$ nm (calculated from the row averages) is in a good agreement with that (˜2 nm) estimated from quasi-elastic light scattering[32]. A common, and here not detailed, conclusion of refs 3 and 32 and of the present work is that the DLVO potential works acceptably well, though one of the outgoing conditions for its derivation (i.e., the condition for linearizing the Poisson−Boltzmann equation[6]) is not met.

3.2.4. Auxiliary Parameters. The parameters C_j, in principle, correct the systematic error made when converting the scattering patterns into absolute units, and thus they are expected to vary around the unity. Because C_j's correlate with the variables appearing in the coefficients of the amplitude(s), for example with the aggregation number and scattering contrast, they may differ from unity for reasons other than wrong normalization. The row-averages of C_j's differ from unity by ~ 5%, suggesting that no serious error was made when converting the scattering patterns into absolute units. The small values of the background correction term ($|B_j| < 4 \cdot 10^{-3}$ cm^{-1}) indicate a precise raw-data treatment, too.

Though the conditions of a rigorous chi-square analysis (the deviations of the theory from the experimental points are fully independent normal random variables, the number n_{dat}, of data points is much greater than n_P, that of the parameters) are not met when fitting SAS patterns, the goodness of the fit is conventionally judged by χ_r^2, the reduced chi-square derived from the sum $\chi^2 = \Sigma_j \chi_j^2$of squared differences as $\chi_r^2 = \chi^2/(n_{dat} - n_P + 1)$. The χ_j^2 data are listed in Table 3 for each pattern; both SANS patterns consist of 33 data points, the SAXS pattern 87 data points. Each model fits the simple SANS spectrum very well; their fitting to the more structured SAXS pattern leads to essentially greater χ_r^2 values. This value significantly decreases if the SANS and SAXS patterns are combined. In all cases, where the SAXS pattern is involved, the 4C model results in much better χ_r^2 data than either the 2S or the 3S model.

4. Conclusions

Two-shell- (2S), three-shell-(3S), and four-component (4C) models have been used to interpret single SANS and SAXS patterns from a 0.0729 **m** D_2O solution of CsDDS, as well as the combination of these patterns. The availability of X-ray data significantly improves the quality of the best-fit values of the model parameters. Comparison of the results from various aspects suggests that the most reliable information on the aggregate structure is obtained when fitting the 4C model to the combined SANS+SAXS patterns. It is pointed out here that using SANS- and SAXS in the same colloidal system is not a new idea: the 2S model, utilized for interpreting single SANS- and SAXS patterns, leads for SDDS micelles to similar results.[37] In this regard, a novel feature of the present work is the fitting of the same model in the same session to the two types of scattering pattern.

The 2S and 3S models are not able to mirror the continuous variations in the spatial distribution of the scattering contrast. Within the limits set by the spatial resolution of the method and by the goodness of the approximation of the model functions, the 4C model is able adequately describe the core- and counterion profiles. Though the poor spatial resolution of the method prevents us from studying the core profile (its thickness falls within the range of π/Q_{max}), the counterion profile could be determined safely: its thickness significantly exceeds the spatial resolution. The model-free, experimental, *p(r)* function is much better approximated by the 4C model than by the 2S model.

A further, favorable, property of the 4C model is its ability to allow insight into the conditions of hydration of the micelles. Because of the incompressibility of the liquid, the spatial distribution of solvent molecules is determined by that of the molecular groups (see ref 4 and section 2.2.2). As discussed in ref 4, this property means that the spatial variation of any colligative thermodynamic quantity around a micelle can be determined from scattering experiments. The 4C results from combined SANS and SAXS patterns show that under optimal conditions some of the molecular volumes can be treated as variable model parameters, providing in the present case a unique method for determining the otherwise unknown mol-(ecul)ar volumes of the headgroup- and counterions.

A common problem of all the three models is that they fail in adequately representing the two scattering patterns for $Q > 2.0$ nm^{-1}. The deviation is obvious; it can also be observed in SANS patterns from sodium alkyl sulfates[3,4] suggesting that there exist molecular correlations in the system which have been disregarded. In ionic micelles, such correlations may be due to

the Coulomb interaction, which forces the headgroups to remain at an equal distance from each other, introducing thus a kind of spatial ordering among them.

Acknowledgment. Support from the National Foundation for Scientific Research, Hungary (OTKA), contract T029958 (Sz.V.), from the Grant Agency of the Czech Republic, contract 203/00/1317 and the Academy of Sciences of the Czech Republic, project Nos. AVOZ4050913 and KSK4050111 (J.P.) is gratefully acknowledged.

Note Added after ASAP Posting. This article was released ASAP on 10/18/2003. Changes were made to ref 2 and the author running head. The correct version was posted on 10/27/2003.

References and Notes

(1) Hayter, J. B.; Penfold, J. *J. Chem. Soc., Faraday Trans. 1* **1981**, *77*, 1851. Hayter, J. B.; Penfold, J. *Colloid Polym. Sci.* **1983**, *261*, 1022.

(2) Kale, K. M.; Zana, R. *J. Colloid Interface Sci.* **1977**,*61*, 312. Vass, Sz. Török, T.; Berecz, E.; Jákli, Gy. *J. Phys. Chem.* **1989**, *93*, 6553.

(3) Vass, Sz.; Gilányi, T.; Borbély, S. *J. Phys. Chem. B* **2000**, *104*, 2073.

(4) Vass, Sz. *J. Phys. Chem. B* **2001**, *105*, 455.

(5) Hayter, J. B.; Penfold, J. *SQHP: a FORTRAN Package to Calculate S(Q) for Macroion Solutions*, ILL Report 80HA07S, Grenoble, 1980. Hayter, J. B.; Penfold, J.; *The Structure Factor of Charged Colloidal Dispersions at any Density*, ILL Report 82HA14T, Grenoble, 1982.

(6) Verwey, E. J. W.; Overbeek, J. Th. G. *Theory of the Stability of Lyophobic Colloids.;* Elsevier: New York, 1948.

(7) Stigter, D. In *Physical Chemistry: Enriching Topics from Colloid and Surface Science*; van Olphen, H., Mysels K. J., Eds.; Theorex, La Yolla, 1975; p 181.

(8) Hansen J. P.; McDonald I. R. *Theory of Simple Liquids*; Academic Press: London, 1976.

(9) Luzzati, V.; Tardieu, A. *Annu. Rev.Biophys. Bioeng.* **1980**, *9*, 1.

(10) Outhwite, C. W.; Bhuiyan, L. B. *Mol. Phys.* **1991**, *74*, 367.

(11) Vass, Sz.; Pleštil, J.; Laggner, P.; Borbély, S.; Pospíšil, H.; Gilányi, T. *Physica B* **2000**, *276*−*278*, 406.

(12) Mukerjee, P.; Mysels, K. *Critical Micelle Concentrations of Aqueous Surfactant Systems*. NSRDS−NBS 36, Washington D. C., 1971.

(13) Hunter, R. J. *Foundations of Colloid Science*, Vols. 1 and 2; Clarendon Press: Oxford, 1989.

(14) Wu C. F.; Chen, S. H.; Shih, L. B.; Lin, J. S. *Phys. Rev. Lett.* **1988**, *61*, 645.

(15) Dreger, E. E.; Keim, G. I.; Miles, G. T.; Shedlowsky, L.; Ross, J. *J. Ind. Eng. Chem.* **1946**, *36*, 610.

(16) Kratky, O.; Pilz, J.; Schmitz, P. J. *Colloid Interface Sci.* **1966**, *21*, 24.

(17) Tartar, H. V. *J. Phys. Chem.* **1955**, *59*, 1195.

(18) Tanford, C. *J. Phys. Chem.* **1972**, *76*, 3020.

(19) Tanford, C. *Proc. Natl. Acad. Sci. U.S.A.* **1974**, *71*, 1811.

(20) Cabane, B.; Duplessix, R.; Zemb, T. *J. Phys.* (*Paris*) **1985**, *46*, 2161.

(21) Vass, Sz. *Struct. Chem.* **1991**, *2*, 375(167).

(22) Bergström, M.; Pedersen, J. S. *J. Phys. Chem.* **1999**, *B103*, 8502. Bergström, M.; Pedersen, J. S.; Schurtenberger, P.; Egelhaaf, S. U. *J. Phys. Chem.* **1999**, *B103*, 9888.

(23) Sears, V. F.; *Thermal-Neutron Scattering Lengths and Cross Sections for Condensed Matter Research*, Report AECL-8940, Chalk River Nuclear Laboratories, Chalk River, Ontario, 1984.

(24) Millero, F. *Chem. Rev.* **1971**, *71*, 147.

(25) One of the authors (Sz. V.) is indebted to Prof. J. S. Pedersen (University of Aarhus, Denmark) for his suggestion aiming at a different but similar approximation.

(26) Israelachvili, J. N.; Mitchell, D. J.; Ninham, B. W. *J. Chem. Soc. Faraday Trans. 2.* **1976**, *72*, 1525.

(27) Mazer, N. A.; Benedek G. B.; Carey, M. C. *J. Phys. Chem.* **1976**, *80*, 1075. Young, C. Y.; Missel, P. J.; Mazer, N. A.; Benedek, G. B.; Carey, M. C. *J. Phys. Chem.* **1978**, *82*, 1375. Missel, P. J.; Mazer, N. A.; Benedek, G. B.; Young, C. Y.; Carey, M. C. *J. Phys. Chem.* **1980**, *84*, 1044. Missel, P. J.; Mazer, N. A.; Benedek, G. B.; Carey, M. C. *J. Phys. Chem.* **1983**, *87*, 1264.

(28) Chen, H.-S. *Physica* **1986**, *B137*, 183.

(29) Feigin, L. A.; Svergun, D. I. Structure Analysis by *Small-Angle X-ray and Neutron Scattering*; Plenum Press: New York, 1987.

(30) Pedersen, J. S.; Posselt, D.; Mortensen, K. *J. Appl. Crystallogr.* **1990**, *23*, 321.

(31) James, F.; Roos, M. *Comput. Phys. Commun.* **1975**, *10*, 373. James, F. *MINUIT Function Minimization and Error Analysis Reference Manual*, Version 94.1, CERN Geneva, 1994.

(32) Corti, M.; Degiorgio, V. *Chem. Phys. Lett.* **1978**, *53*, 237. Corti, M.; Degiorgio, V. *J. Phys. Chem.* **1981**, *85*, 711.

(33) Glatter, O. In *Small-Angle X-ray Scattering*; Glatter, O., Kratky, S., Eds.; Academic Press: London, 1982; p.167.

(34) Glatter, O. *J. Appl. Cryst.* **1977**, *10*, 415.

(35) Vass, Sz. *Acta Cryst.* **1998**, *A54*, 249.

(36) Vass, Sz.; Pleštil, J.; Borbély, S.; Gilányi, T.; Pospíšil, H. *J. Mol. Liquids* **1997**, *72*, 69.

(37) Zemb, T.; Charpin, P. *J. Physique* **1985**, *46*, 249.